Quantitative assessment of a threshold for risk mitigation actions

Theodore H. Sweetser[(1)], Barbara M. Braun[(2)], Michael Acocella[(3)], and Mark A. Vincent[(4)]

[(1)] Jet Propulsion Laboratory, California Institute of Technology, 4800 Oak Grove Dr. Pasadena, CA, USA 91109
[(2)] The Aerospace Corporation, 2155 Louisiana Blvd. NE, Suite 5100, Albuquerque, NM, USA 87110
[(3)] Northrop Grumman, 45101 Warp Dr., Dulles, VA, USA 20166
[(4)]Raytheon, 2810 Colby Dr., Boulder, CO 80305

ABSTRACT

Many low-Earth-orbit missions have a policy that if a future conjunction with a secondary object such as a piece of orbital debris is detected, a go/no go meeting will be held to decide about a risk mitigation action before the time of closest approach. Commonly, the policy is that a probability of collision (Pc) above a predetermined action threshold at the time of the meeting means the mission will take action to reduce the risk. The value to which the action threshold is set is a compromise—if it is higher, then there is a higher probability that a collision might occur when action is not taken; if it is lower, then more actions will be taken, increasing the cumulative costs and risks of the actions themselves. This paper shows how a policy using an action threshold affects the overall mission risk of a collision with a large object. We augment this with estimates of action success, expected hard-body radius, and expected covariance to obtain an algorithm for estimating the risk reduction associated with an action threshold policy. We apply this algorithm to the OCO-2 and CloudSat missions as examples, using historical conjunction data for these two missions, and show how this algorithm can guide developing missions in setting an action threshold.

1 INTRODUCTION

The risk that any Earth-orbiting spacecraft will collide with an object in space is low—NASA requires that every space mission show that there is less than one in a thousand chance of a collision over the entire time in orbit before it will be allowed to launch. But the risk is always increasing, and with proposals being pursued to launch thousands of spacecrafts for some missions the concern about the risk is increasing even faster.

One approach to reducing risk is simply to think small—a smaller cross-section has a lower chance of being hit. But this is not often a feasible approach. Many Earth-orbiting missions have adopted a more active strategy and have established a process to dodge away from any orbiting object (the secondary) that is predicted to come too close to the mission spacecraft (the primary). This generally involves performing a maneuver to change the orbit of the primary, but can also be done by changing or delaying a maneuver that was planned for other purposes, e.g., an inclination adjustment or for drag make-up, but that puts the primary in harm's way.

Either way, the necessary first step is detecting the threat. This involves not only noticing that an object is going to pass nearby, i.e., will be in conjunction, but also evaluating the risk posed to see if it is high enough to be worth taking action, which is operationally expensive and poses risks of its own. Almost always this evaluation is done by measuring the estimated probability of a collision, traditionally denoted Pc, against an action threshold, T_a—if $\mathrm{Pc} > T_a$ then action will be taken, either a maneuver will be performed or an otherwise already-planned maneuver will be modified. The setting of the action threshold is a policy decision on the part of a mission project. This paper presents a method for quantifying the effect of using the action threshold to help the mission set the value of T_a.

This study is not the first to address the issue of setting the action threshold. Several studies have been done using a variety of approaches. Often these have attempted to quantify the overall risk and the mitigated risk, which requires a model of the population of objects in orbit. Some studies have assumed that a conjunction is happening and focused on methods to measure the risk of that conjunction given just an estimated miss vector. Many studies have turned the problem around and focused on quantifying the chance that a collision will not be detected, i.e., that Pc will be less than T_a but that nevertheless a collision happens—this is called the missed-detection problem. Our study concentrates on the risk reduction aspect; we estimate the fraction of overall risk that is mitigated as a function of T_a, independent of particular conjunctions or what the actual risk is.

2 MISSED DETECTION STATE OF THE ART

Foster and Estes's paper in 1992 [1] was an early and seminal study to address this issue. They take the approach of calculating the actual risk to the mission and the actual risk removed by mitigation actions; they use flux models to quantify the relationships in a triad of maneuver thresholds, residual risk and maneuver rates.

The analysis of Foster and Stansbery [2] looked at a different region of space for the International Space Station (ISS) and Space Shuttle (STS) than the analysis presented here for satellites in the A-Train Constellation. They binned secondary objects according to the uncertainty in their orbits, similar to the binning shown in Section 7 below. Thus, their 15 bins and our 19 bins correspond to a different-sized ellipse in the conjunction plane for a fixed threshold (see Section 5). Their overall results were also similar to ours: a threshold of $1x10^{-4}$ produced a residual risk of about 20% with a few maneuvers needed per year. There was one exception for the STS when a threshold of $3x10^{-5}$ was more appropriate, but of course doing an avoidance maneuver with the shuttle is in some ways simpler than moving a satellite in the A-Train.

Sanchez-Ortiz *et al*. [3] looked at risk thresholds and the resulting risk reductions and number of maneuvers for a low-Earth-orbit satellite (Envisat), the ISS, and geosynchronous and geosynchronous-transfer orbits. The results for the first is most applicable for comparisons to the results in this paper, though there has to be some translation since they plot number of maneuvers vs. risk threshold and then risk reduction vs. number of maneuvers. They also produced numerical results using a European flux model named MASTER.

Chan's textbook [4] contains explanations of several of the formulas used here. In particular, in Chapter 4 he introduces the simple formula (Equation 5 here). He also introduces the Rician integral [5] with a simplified solution in the form of a truncated series expansion to calculate the 2-D Pc. He notes that if the miss distance is zero then the Rician integral becomes the Rayleigh integral which has a closed-form solution. Plus, in Chapter 12 he creates an annual probability of collision for a reference satellite at 618 km altitude which can be compared to the flux models used by others.

Carpenter *et al.* [6] used statistical methods, in particular the Wald Sequential Probability Ratio test, with both a frequentist and Bayesian approach to test the two hypotheses: whether there will be a collision or whether there will not be collision. Notable is that the test, which is based on the entire observation history for a future conjunction, can support either hypothesis or neither, and in the latter case suggest more observations are needed. In this strategy, the thresholds for doing a maneuver (when the test supports a collision hypothesis) or dismissing the conjunction without a maneuver (when the test supports a non-collision hypothesis) depend on *a priori* values considered acceptable for the probabilities of a missed detection and of a false alarm. Their assertion is that this is a better strategy than the action threshold strategy being examined here.

Alfano and Oltrogge [7] present relationships between Mahalanobis space and Pc. These relationships are then used to derive bounding values for false alarms (Type I errors) and missed alarms that result in a collision (Type II errors), the latter of which is the subject of this paper. However, they use a somewhat more complicated formula to relate a Pc threshold to a Mahalanobis distance threshold (the latter is called dm_{alert} in their paper, but r_M in this paper) than is used by us. The 17th figure in their paper is the probability of being outside a given Mahalanobis screening threshold, which can be compared to Eq. 4 below.

The origin of the analysis presented in Vincent and Sweetser [8] came from the question: "how much credit should be given to doing risk mitigation maneuvers when calculating the mission lifetime probability of being hit by large objects for End of Mission requirements." The analysis then focused on the probability of detecting and mitigating a conjunction that was actually going to be a collision. That analysis is presented in this paper in Sections 4 and 5. A side benefit of that analysis was its application to a previously-developed tool named PC4 [9, 10]. It uses the current probability density function (PDF) along with a model of what the covariance (at Time of Closest Approach – TCA) would be from a future observation of the secondary object to calculate the likelihood that the future Pc will cross a chosen threshold. As it turns out, if the miss distance is chosen to be zero and the future covariance is modelled to be the same as the current one, this likelihood turns out to be the probability of detection as derived in Section 5.

3 SOME BASIC STATISTICAL CONCEPTS

These basic concepts are given to establish our notation and recall those concepts that are used in the development. We use boldface to represent multidimensional variables, such as vectors and matrices; capital letters are used for random variables and for matrices.

3.1 Multivariate normal distributions

For our purposes, we consider multivariate normal distributions that are full-rank affine transformations of a standard normal random vector of the same dimension. Thus $\boldsymbol{X} = (X_i), i = 1\ to\ n$, is a multivariate normal distribution of dimension n here if and only if $\boldsymbol{X} = \boldsymbol{x}_0 + \boldsymbol{TS}$, where $\boldsymbol{T}$ is a matrix with non-zero determinant and $\boldsymbol{S}$ is the vector (S_i) of the same dimension as $\boldsymbol{X}$, where each S_i is a random variable that is normally distributed with mean 0 and variance 1. The matrix $\boldsymbol{Z} = \boldsymbol{TT}^{\mathsf{T}}$ is the covariance matrix of $\boldsymbol{X}$ and is positive definite here by definition, where the superscript operator T stands for "transpose" (and -T means "inverse transpose"). The probability density function (PDF) f for a point $\boldsymbol{x}$ is

$$f(\boldsymbol{x}) = 1/\sqrt{(2\pi)^n |\boldsymbol{Z}| e^{(\boldsymbol{x}-\boldsymbol{x}_0)^{\mathsf{T}} \boldsymbol{Z}^{-1} (\boldsymbol{x}-\boldsymbol{x}_0)}} \tag{1}$$

where $\boldsymbol{x}_0$ is the mean of the n-dimensional random vector $\boldsymbol{X}$. The square root of the determinant of $\boldsymbol{Z}$ is just the determinant of $\boldsymbol{T}$, which is the scaling factor for the change in volume that happens when the transformation $\boldsymbol{T}$ is applied; it is this scaling factor division which keeps the integral of the PDF over the space equal to 1 and also preserves the cumulative distribution over a volume, i.e., the cumulative distribution over a region in the space of the standard normal random vectors is the same as the cumulative distribution over the image of that region by $\boldsymbol{T}$ in the multivariate normal vector space. There is no closed-form general formula for calculating a cumulative distribution value for different volumes within the distribution space, but such a formula does exist for volumes within any fixed Mahalanobis distance of the mean vector.

3.2 Mahalanobis distance

In our space navigation work we typically characterize multivariate distributions by considering ellipsoids (ellipses in two dimensions) centered at the mean point and representing one sigma, two sigma, etc., distances from the mean. Figure 1 shows this for a typical conjunction. These ellipsoids are the images under the mapping $\boldsymbol{T}$ of the integer radius spheres (circles) in the standard normal random vector space. On these ellipsoids, as on their preimages, the value of the PDF is constant, as is their distance from the origin in the preimage. This distance in the standard normal vector space gives what is called the Mahalanobis distance [11] in the multivariate vector space, which is defined this way for any point in the multivariate vector space. More explicitly the Mahalanobis distance $r_M(\boldsymbol{x})$ of a point $\boldsymbol{x}$ from the mean $\boldsymbol{x}_0$ in the multivariate vector space is given by.

$$r_M(\boldsymbol{x}) = \|\boldsymbol{T}^{-1}(\boldsymbol{x} - \boldsymbol{x}_0)\| = \sqrt{(\boldsymbol{x} - \boldsymbol{x}_0)^{\mathsf{T}} \boldsymbol{Z}^{-1} (\boldsymbol{x} - \boldsymbol{x}_0)}. \tag{2}$$

Note that this lets us write the PDF for $\boldsymbol{x}$ (see Eq. 1) as

$$f(\boldsymbol{x}) = 1/\sqrt{(2\pi)^n |\boldsymbol{Z}| e^{r_M(\boldsymbol{x})^2}}. \tag{3}$$

One characteristic of the Mahalanobis distance is that the distribution of the Mahalanobis distance from the mean is a chi distribution whose number of degrees of freedom is the dimension of $\boldsymbol{X}$, since the Mahalanobis distance is the distance in the standard normal random distribution. In two dimensions this means that the cumulative distribution inside the distribution ellipse for any r_M is given by the Rayleigh distribution (which is a chi distribution with two degrees of freedom) with unit scale parameter. Thus the cumulative distribution function (CDF) $F(r_M)$ relative to the mean, i.e., the probability of being within an r_M-ellipse in Fig. 1, is just

$$F(r_M) = 1 - e^{-({r_M}^2/2)}. \tag{4}$$

4 MISS DISTANCE AND PROBABILITY OF COLLISION

We call the vector from the primary body (our spacecraft) to the secondary body (an object passing nearby) at the closest approach of the secondary to the primary the *miss vector*. We have a collision if the volume of the secondary body intersects the volume of the primary body along the relative trajectory, either at or just before or after the closest approach. To simplify our analysis, we approximate this situation by combining the two body volumes into a sphere centered at the primary body; then if the miss vector is inside the combined volume we take that to be a collision, and Pc is the integral of the PDF over the combined volume.

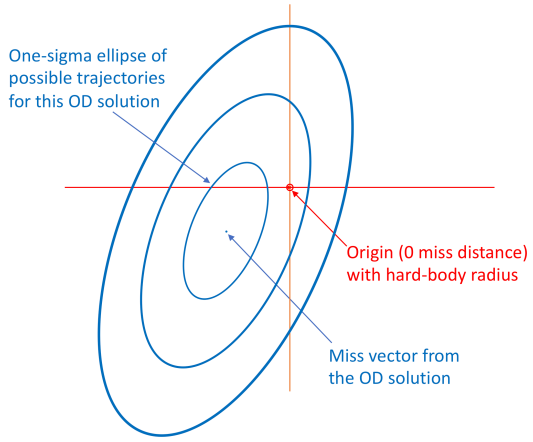

Fig. 1. The distribution of errors in the estimate of the miss vector, relative to the estimate, is the same as the distribution of possible true miss vectors given this estimated miss.

To better visualize and to simplify this situation, we map it into the conjunction plane, which has just two dimensions. The *conjunction plane* is a plane perpendicular to the relative velocity vector at the miss vector; since the miss vector is at the point of closest approach, the conjunction plane contains both the secondary and the primary body. We coordinatize the conjunction plane by placing the origin at the primary body and choosing perpendicular axes in the plane, usually by making the "vertical" axis (when drawing the plane) as the most radial axis in the plane, so that the "horizontal" axis is truly horizontal with respect to the Earth. Alternative coordinatizations choose the x-axis to include the miss vector, or align the x-axis with the semi-major axis of the error ellipse.

Now we have the situation shown in Fig. 1. We approximate the covariance of the estimated miss vector by taking the sum of the covariances of the estimated positions of the primary and secondary bodies and then projecting that onto the conjunction plane. The region of interest is the circle centered at the origin and with radius equal to the combined hard-body radius r_{HB}—if the actual miss vector is within this circle then we consider that to be a collision. As above, Pc is equal to the integral of the PDF over the area of this circle.

Foster and Estes's seminal paper in 1992 [1] is widely attributed to be the first to describe the above method for reducing the calculation of Pc values to 2-D. For the actual calculation they gave two algorithms—one uses the Monte Carlo method and the other simply calls for numerically integrating the PDF function (though the formula they give for the PDF function depends on using coordinates in the conjunction plane that are aligned with the principal axes of the error ellipse). The boundary of the area of the combined hard body is described in polar coordinates, which are used for the numerical integration.

Subsequent authors [12, 13] have implemented various quadrature methods to do the same numerical integration. Chan [4] has proposed analytical techniques and Alfano [12] compared them against the numerical methods for computational speed and accuracy.

In particular, Carpenter [6] (following Chan [4]) has proposed using an ellipse instead of a circle to represent the combined hard body, where the ellipse is similar in shape and orientation to the error ellipse but has the same area as the circular representation; the cumulative distribution over this ellipse is given by the Rice distribution [5], which gives the value of the CDF as an infinite sum involving modified Bessel functions.

In this study we use a much simpler approximation (called Method 1 in [8]): we simply multiply the value of the PDF at the center of the circle (i.e., the origin in Fig. 1) by the area of the circle, which is $\pi {r_{HB}}^2$, thus

$$\mathrm{Pc} = \pi {r_{HB}}^2 / \sqrt{(2\pi)^2 |\boldsymbol{Z}| e^{r_M(\boldsymbol{x})^2}}. \tag{5}$$

The compelling advantage of this approximation is shown in the next section. Chan (Chapter 4, [4]) warns of the limitations of this approximation, though in general it is a reasonable approximation if the r_{HB} is small compared to the covariance. For example, in the isotropic case, where $|\boldsymbol{Z}| = \sigma^2$, Eq. 5 gives the highest overestimate of Pc when $\boldsymbol{x}$ is the origin because the curvature of the surface is maximum there, but this maximum overestimate is less than 1% when $r_{HB} < 0.2\sigma$. Two significant digits of precision are sufficient in the following analysis.

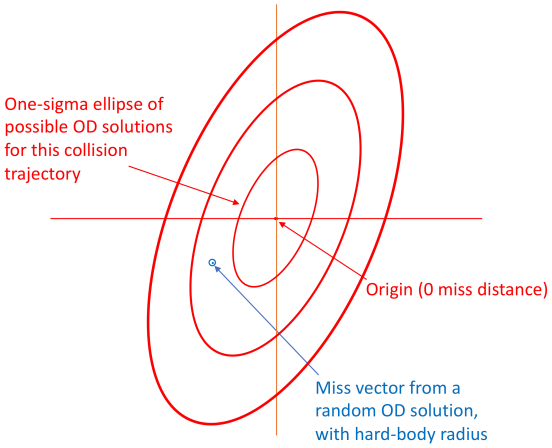

Fig. 2. This distribution of possible OD solutions assumes that the true miss distance is zero.

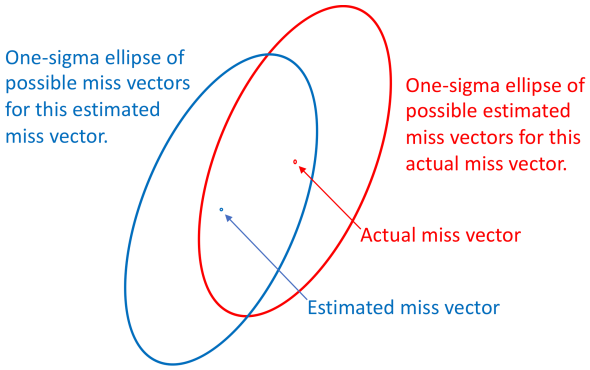

Fig. 3. There is a symmetry between possible miss vectors for a given estimate and possible estimates for a given miss vector—the distributions are the same.

5 PROBABILITY OF DETECTION

In Section 4 we considered the probability of collision given an estimated miss vector, i.e., the probability that the true miss vector is within the combined hard-body radius. Now we turn that problem upside down: given that we are on a collision course, what is the probability that the estimated miss vector will have a Pc above the action threshold? This situation is illustrated in Fig. 2.

Note that the covariance of the distribution of possible miss vectors in Fig. 2 is derived from the covariances of the primary and secondary orbit distributions, and is the same as the distribution of errors in the estimate of a miss vector—indeed this is the source of the error distribution. This symmetry is illustrated in Fig. 3. Thus the value of the Pc for any particular estimated miss vector is equal to the cumulative distribution over the area of the combined hard body centered on the estimated miss vector, which is shown in blue in Fig. 2.

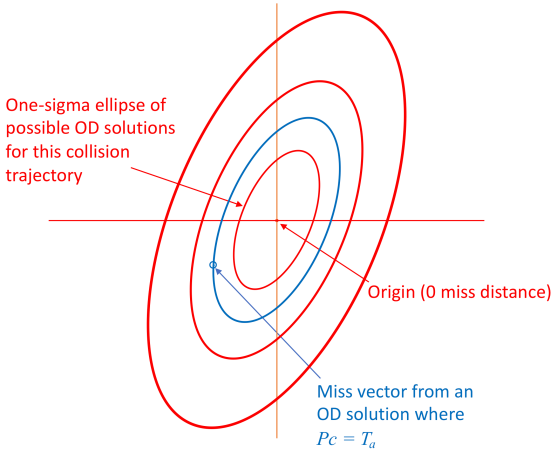

Fig. 4. If the latest estimate of the miss vector is within the mission's action threshold ellipse (in blue), then some action will be taken to mitigate the risk.

Now consider the region on the conjunction plane where Pc is greater than the action threshold value. The cumulative distribution of possible miss vectors over this region gives the probability that the Pc for the estimated miss vector for this conjunction will be equal to or greater than the action threshold, given that the true relative trajectory is a collision. This is traditionally called the probability of detection, although "probability of threat recognition" would be better since it depends on the action threshold chosen.

Now the significance of our choice of method for approximating Pc becomes apparent. In the conjunction plane, and given a particular distribution covariance, if Pc depends only on the PDF value at the center of the combined hard body, then contours of constant PDF are also contours of constant Pc, which are contours of constant r_M. This is illustrated in Fig. 4. And we know how to calculate the cumulative distribution within an r_M-ellipse such as the blue ellipse in Fig. 4—it is given in Eq. 4.

We have assumed here that the miss vector is zero, i.e., that the collision is dead center. What if the collision is off-center, or even at the edge of the hard-body radius? Then the ellipse is shifted and a slice of a higher PDF region on one side is replaced by a lower PDF region on the other side. We have used numerical approximations of the CDFs for centered and shifted ellipses for $T_a = 0.0001$ and for various values of r_{HB}. From these results we estimate that the centered ellipse overestimates the CDF by much less than 1% when $r_{HB} < 0.2\sigma_b$, where σ_b is the semi-minor

axis of the error ellipse in the conjunction plane; this is the same limit that bounds the error in the approximation of Pc to be less than 1%, as shown in Section 4.

6 QUANTIFYING THE RISK MITIGATED

We are now prepared to find out how much a strategy of risk mitigation using an action threshold actually reduces risk. The fraction of risk removed is the product of four factors: the probability that the threat will be noticed and analyzed; the probability of detection given an analyzed threat and a predetermined action threshold; the probability of a mitigating action being successfully taken; and the fraction of risk that the action risk removes.

Given current orbital tracking capabilities and the large volume examined for conjunctions around each satellite, a conservative estimate of the probability that a threat will be noticed is 99%. Operational experience with satellites that do risk mitigation indicates that 90% is a conservative estimate that a mitigation action will be successful. (See Sections 7 & 8 below for specific examples.) And if we require that an action be designed to reduce the risk by at least two orders of magnitude, then the fraction of risk removed by the action is at least 99%. This leaves the probability of detection to be determined.

Suppose now that a project has determined or chosen values for r_{HB}, the combined hard-body radius, T_a, the action threshold, and Z_E, the expected value of $|\boldsymbol{Z}|$, the determinant of the covariance, which for orbit determination depends on the partial of the state with respect to navigation data measurement error and the size of those errors expected given the equipment making the navigation data measurements. Then we can use Eq. 5 to solve for the r_M that gives the boundary of the region in which the Pc is greater than T_a as follows:

$$r_M = \sqrt{-\ln\left((2\pi)^2 |\boldsymbol{Z}| \left(\frac{T_a}{\pi {r_{HB}}^2}\right)^2\right)}. \tag{6}$$

Now we can use that expression for r_M in Eq. 4 to get P_D, the probability of detection:

$$P_D = 1 - e^{-\frac{1}{2}\left(-\ln\left((2\pi)^2 |\boldsymbol{Z}| \left(\frac{T_a}{\pi {r_{HB}}^2}\right)^2\right)\right)},$$

which is

$$P_D = 1 - \sqrt{\left((2\pi)^2 |\boldsymbol{Z}| \left(\frac{T_a}{\pi {r_{HB}}^2}\right)^2\right)}. \tag{7}$$

This can be simplified further. If σ_a and σ_b are the semi-major and semi-minor axes of the error ellipse for the covariance, then $|\boldsymbol{Z}| = {\sigma_a}^2 {\sigma_b}^2$ and we have the following surprisingly simple formula:

$$P_D = 1 - 2T_a \frac{\sigma_a \sigma_b}{{r_{HB}}^2}. \tag{8}$$

Note that if $|\boldsymbol{Z}|$ is too large, P_D becomes negative, which is impossible; this just means that r_M in Eq. 6 was imaginary, which happens if there is no r_M at which Pc is equal to or greater than T_a, even if the object is on a direct collision course with the satellite. In such a situation P_D is actually zero.

Unfortunately, there is no single covariance that applies for all conjunctions—instead there is a wide range of covariances. In the cases we examine below, the average value of $|\boldsymbol{Z}|$ is large enough that the P_D is unrealistically small. So instead we take a divide-and-conquer approach.

To calculate the overall risk reduction, we assume a distribution of the values of $|\boldsymbol{Z}|$ for each satellite and represent that as a histogram by binning the values of $|\boldsymbol{Z}|$ into logarithmic bins from 10^1 to 10^{19} and estimating a frequency of

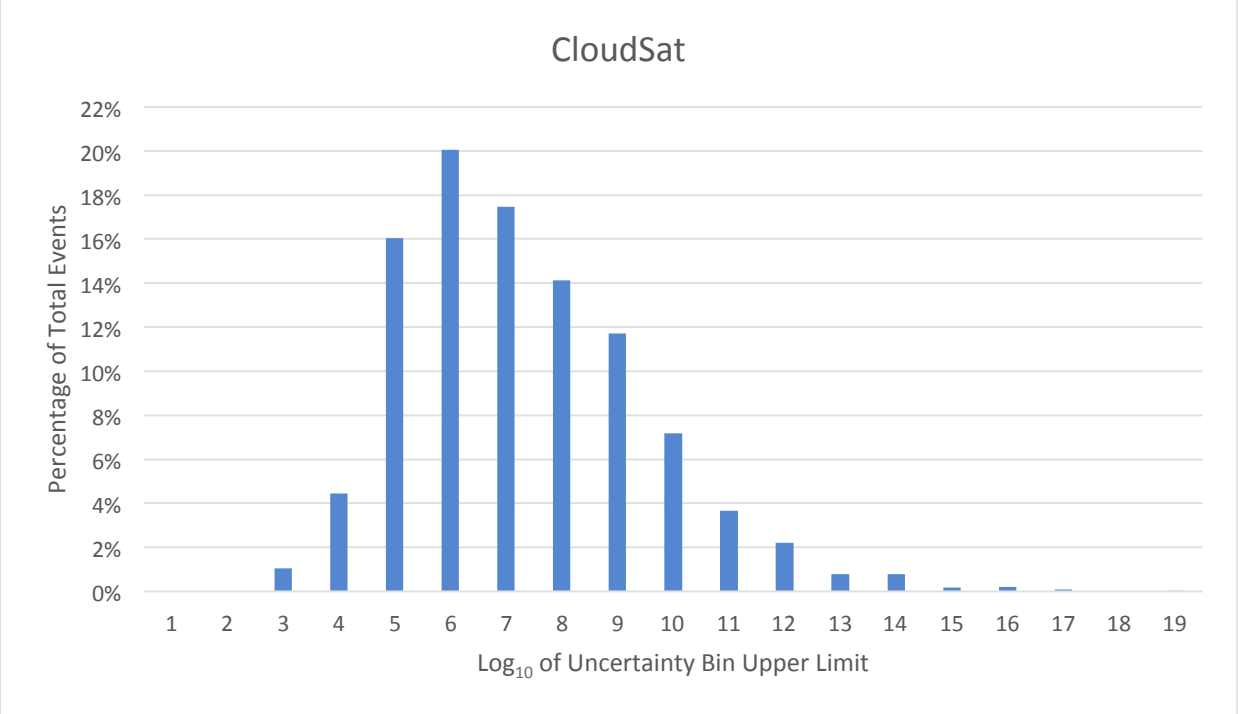

Fig. 5. Histogram of the determinants of the 2-D covariance matrix for 2323 conjunctions experienced by CloudSat from 2015-04 through 2019-09.

occurrence of values of $|\boldsymbol{Z}|$ in each bin. Then, we used the upper bound of each bin in Eq. 8 to compute the P_D for that bin, which is zero when $|\boldsymbol{Z}|$ is so large that P_D is zero.

Finally, we multiplied the risk capture of each bin by the percentage of total events that fell into each bin, and summed the results over all bins to determine the overall risk capture.

7 RISK MITIGATION FOR CLOUDSAT

To estimate the risk reduction over time for the space environment experienced by CloudSat, we began by computing the value $|\boldsymbol{Z}|$ based on the uncertainty reported in the last report for each conjunction that arrived at least 24 hours before TCA. From this report, we used the size of semi-major and semi-minor axes of the one-sigma uncertainty ellipse, squared, which is the variance in each principal axis of the probability distribution. The product of these two values is the value $|\boldsymbol{Z}|$ in Eqs. 1 & 3. Given a hard body radius $r_{HB} = 3.5$ m and an action threshold $T_a = 0.0001$ for CloudSat, the Mahalanobis radius r_M can be calculated using Eq. 3. The risk captured can then be calculated from the action threshold Mahalanobis radius by using Eq. 4. However, this gives the risk captured only for conjunctions which have that value for $|\boldsymbol{Z}|$, and not for the overall risk reduction inherent in the maneuver approach.

To calculate the overall risk reduction, we created a histogram of the values of $|\boldsymbol{Z}|$ for CloudSat over the period of time examined. We binned the values of $|\boldsymbol{Z}|$ into logarithmic bins from 10^1 to 10^{19} and calculated the frequency of occurrence of values of $|\boldsymbol{Z}|$ in each bin. Then, we used the upper bound of each bin in Eq. 3 to compute the Mahalanobis radius and the risk capture for that bin. As the value of $|\boldsymbol{Z}|$ increases (i.e., as the combined uncertainty grows larger), the value in the radicand of Eq. 3 becomes negative, and no real solution for the risk capture exists. This represents the situation where the uncertainty is so large that the probability of collision will never reach the action threshold value, even if the object is on a direct collision course with CloudSat. In this case, the risk capture is zero, and a zero percent risk reduction was entered for that bin.

Finally, we multiplied the risk capture of each bin by the percentage of total events that fell into each bin, and summed the results over all bins to determine the overall risk capture. The data for this calculation for CloudSat are given in Fig. 5, and the resulting percent likelihood of detection is 75.2%. We then consider the likelihoods of

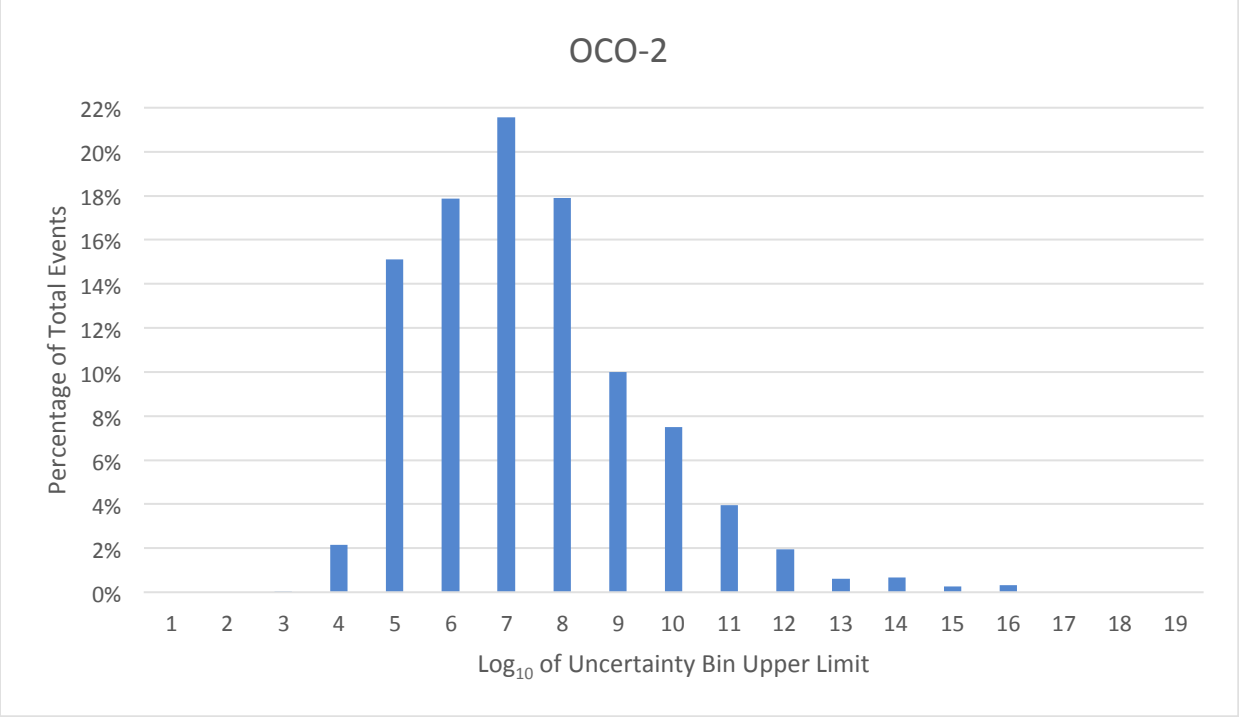

Fig. 6. Histogram of the determinants of the 2-D covariance matrix for 2402 conjunctions experienced by OCO-2 from 2015-01 through 2019-09.

noticing the conjunction and performing the mitigation action, and factor in the amount of risk reduction from the mitigation. CloudSat has had six failed maneuver attempts out of 230 attempts, giving a 95% confidence interval of 0.95 to 0.99 for the probability of success, using the normal approximation method of finding the confidence interval. Using the lower end of the confidence interval, the result is a total risk reduction estimate of 70%.

8 RISK MITIGATION FOR OCO-2 AND OTHER A-TRAIN SATELLITES

The same methodology was applied to OCO-2, which has a hard-body radius of 6 m and the same action threshold as CloudSat, 0.0001. The data for this calculation for OCO-2 are given in Fig. 6, and the resulting percent likelihood of detection is 84.7%, which is larger than CloudSat's because the combined hard-body radius is larger. Table 1 gives the likelihood of detection using this method for a whole suite of A-Train and C-Train satellites. The second major contributor to the estimate of risk reduction is the likelihood of succeeding to perform the planned mitigation action. OCO-2 has attempted to make 57 maneuvers in orbit with no failures; the mission deferred two of the maneuvers to avoid conjunctions, which counts as successful risk mitigation actions, so the 95% confidence interval for the probability of a successful maneuver is from 0.98 to 1.0 by the Clopper-Pearson interval definition. For OCO-2 this means a total risk reduction estimate of 81%.

9 SETTING AN ACTION THRESHOLD FOR NEW MISSIONS

No organizational-level standards currently exist for setting operational action thresholds for on-orbit collision risk mitigation. Lifetime probability of collision limits, however, do exist in a number of agency regulations; for example, NASA Technical Standard 8719.14B, *Process for Limiting Orbital Debris*, states the probability of accidental collision with space objects larger than 10 cm in diameter may not exceed 0.001 for satellites passing through low earth orbit. The techniques described in this paper can help new missions set action thresholds based on these lifetime probability of collision requirements.

To accomplish this, a new mission would need an estimate of not only the debris flux expected for its orbital environment, but also the typical distribution of uncertainties. As an example, Fig. 7 shows that distribution for five

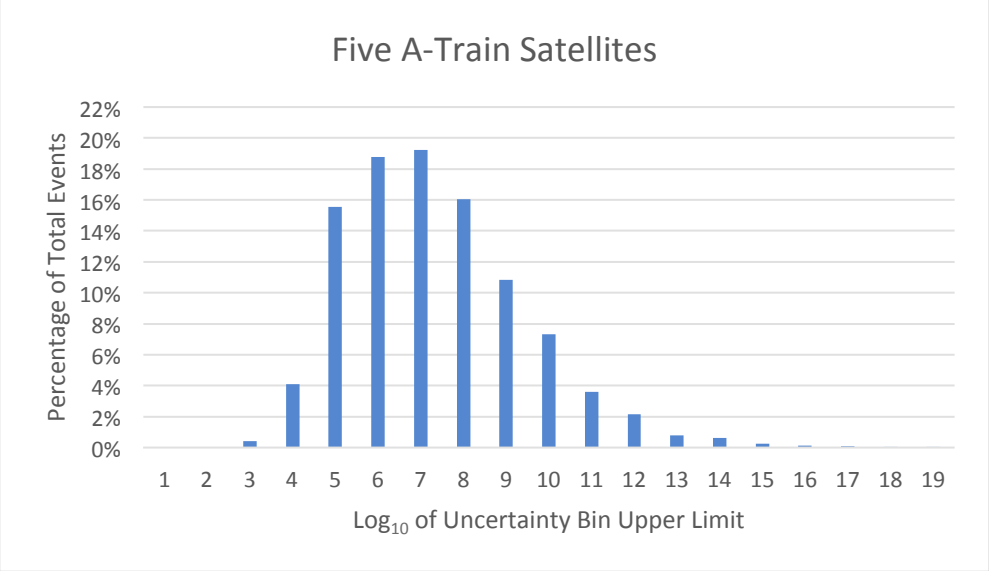

Fig. 7. Histogram of the determinants of the 2-D covariance matrix for 10,316 conjunctions experienced by Aqua, Aura, CloudSat, CALIPSO, and OCO-2 between 2015-01 and 2019-09.

satellites in the A-Train and C-Train orbits, which are sun-synchronous at approximately 700km altitude; compare this inclusive plot to Figs. 5 & 6 to see how distributions for individual missions can vary. These individual distributions give the results shown in Table 1, which depend almost entirely on the combined hard-body radius that applies to each mission. We expect this distribution pattern of covariances to apply for any sun-synchronous orbiter, but the pattern for spacecraft at different inclinations could be different.

Missions would accomplish an initial calculation of lifetime probability of collision based on the overall debris flux using current tools (i.e., NASA's Debris Analysis Software and similar tools). Should the results of this analysis (which takes into account the different stages of a satellite's lifetime, from launch through operations and disposal) indicate a lifetime probability of collision that meets organizational requirements, the satellite would theoretically be done; no collision-avoidance maneuvers would be required by this regulation. As discussed elsewhere [8], however, in practical applications the situation is more complicated.

Should this calculation result in a violation of the lifetime limit – or should the mission's program management or organizational leadership desire a stricter limit – the mission could determine an action threshold using the techniques described in this paper. With an estimate of the uncertainties of the debris crossing through its operational orbit, the mission could calculate, based on its hard-body radius and proposed action threshold, the percentage of the risk that would be reduced through mitigation actions during its operational lifetime. The residual risk would be added to the probability of collision calculated during the satellite's non-operational lifetime (the period of time, for example, following passivation when no maneuvers are possible) to provide a new lifetime

Table 1. Probabilities of detection for five A-Train and C-Train sun-synchronous orbiters at about 700 km altitude.

Satellite	Hard Body Radius	Threshold	Estimated Detection Rate P(Pc > T)	Data Span	Number of Reports	Number of Days
CloudSat	3.5	1.00E-04	75.2%	Apr 2015 - Sep 2019	2323	1632
CALIPSO	14.8	1.00E-04	92.5%	Jan 2015 - Apr 2019	2261	1586
Aqua	20	1.00E-04	96.3%	Jun 2016 - Apr 2019	1560	1047
Aura	20	1.00E-04	96.6%	Jun 2016 - Apr 2019	1772	1045
OCO-2	6	1.00E-04	84.7%	Jan 2015 - Sep 2019	2402	1720

probability of collision number that meets the standard. This action threshold would become the on-orbit operational action threshold for risk mitigation. To ensure a conservative analysis, missions would also likely factor in an estimate of the likelihood of a risk mitigation maneuver being performed successfully.

10 SUGGESTIONS FOR FUTURE WORK

Equation 8 depends on two significant approximations: that we can estimate probability of collision by taking the PDF at the center to be the average of the PDF over the combined hard-body radius, and that the probability of detection for any point in the hard-body radius is very close to the value for the center of the hard body. We have some evidence that these assumptions give over-estimates that are much less than 1% for combined hard-body radii that are less than 0.2 times the smaller sigma in the covariance (the semi-minor axis of the error ellipse). The relationship between the approximation error and the size of the combined hard body deserves a closer look.

Another area of study is the further application of the above methodology to data from operational missions. Estimates of the actual risk and risk mitigated for the missions considered above can be made and distributions of the covariances for missions in other orbits could be determined.

11 ACKNOWLEDGEMENTS

The work described in this paper was carried out in part at the Jet Propulsion Laboratory, California Institute of Technology, under a contract with the National Aeronautics and Space Administration. The authors thank NASA Goddard Space Flight Center's Conjunction Assessment Risk Analysis (CARA) team for providing covariance data.

12 REFERENCES

1. Foster, J.L. and Estes, H.S., "A Parametric Analysis of Orbital Debris Collision Probability and Maneuver Rate for Space Vehicles," NASA JSC 25898, August 1992.
2. Foster, J. and Stansbery, E.G. Fundamentals of debris collision avoidance, in: Proceedings of the 54th International Astronautical Congress, Paper IAC-03-IAA.5.3.03, September 29–October 3, 2003.
3. Sanchez-Ortiz, N., Bello-Mora, M. and Klinkrad, H., Collision avoidance manoeuvres during spacecraft mission lifetime: Risk reduction and required DV, Advances in Space Research 38 pp. 2107-2116, 2006.
4. Chan, F.K Spacecraft Collision Probability, The Aerospace Press, 2008.
5. Rice, S.O. "Mathematical Analysis of Random Noise," Bell System Tech. Journal, 23, 282-332, 1944.
6. Carpenter, J.R. Markley, F.L. and Gold, D., "Sequential Probability Ratio Test for Collision Avoidance Maneuver Decisions," Journal of the Astronautical Sciences, Vol. 59, pp. 273–286, Nos. 1–2, Jan.–June 2012.
7. S. Alfano and D. Oltrogge, "Probability of Collision: Valuation, variability, visualization, and validity," Acta Astronautica, Vol. 148, pp. 301-316, July 2018.
8. Vincent, M.A. and Sweetser, T.H, "A New Look at Predictive Probability of Collision, Predictive Maneuver Trade Space and the Probability of a Missed Mitigation," Proc. of the 2019 Astrodynamics Specialist Conference Portland, ME, August 11-15, 2019.
9. Vincent, M.A., "Bridging the gap between academia and operations for orbital debris risk mitigation," Proc. Of the Advanced Maui Optical and Space Surveillance Technologies Conference, Sept. 15-18, 2015.
10. Vincent, M.A." Paving the bridge between academia and operations for orbital debris risk mitigation," Proc. Of the Advanced Maui Optical and Space Surveillance Technologies Conference, Sept. 20-23, 2016.
11. Mahalanobis, P.C., "On the generalised distance in statistics," Proc. of the National Institute of Sciences of India., Vol. 2 (1), 1936.
12. Patera, R.P., "General Method for Calculating Satellite Collision Probability," AIAA Journal of Guidance, Control, and Dynamics, Vol. 24, Number 4, pp. 716-722, July-August 2001.
13. S. Alfano, S., "Review of Conjunction Probability Methods for Short-term Encounters," Advances in the Astronautical Sciences, 127 pp. 719-746, 2007.